Modeling of Air Separation in a LSCF Hollow-Fiber Membrane Module

Xiaoyao Tan and K. Li
Dept. of Chemical Engineering, University of Bath, Claverton Down, Bath, BA2 7AY, UK

Mixed ion-conducting ceramic membranes are promising in oxygen separation from air due to their infinite permselectivity. Hollow-fiber-shaped membranes can provide a high surface area for such an application. A mathematical model for a hollow-fiber $La_{0.6}Sr_{0.4}Co_{0.2}F_{0.8}O_{3-\delta}$(LSCF) membrane module for air separation was developed and a performance of the module at various operating conditions was studied theoretically. The simulation results reveal that the cocurrent is a better operating flow pattern than the countercurrent flow pattern. The vacuum operation on the lumen side of the membrane module is preferable to the elevated pressure operation on the shell side for achieving high oxygen productivity. A high vacuum level and a desired membrane area are essential to produce the pure oxygen and nitrogen simultaneously. Experimental results and kinetic parameters in the literature obtained from the LSCF membrane for air separation agreed satisfactorily with the theoretical solutions.

Introduction

Mixed conducting oxides exhibit both ionic and electronic conductivities. When an oxygen partial-pressure differential is imposed across a dense membrane made from these oxides at high temperatures, oxygen is permeated in a form of oxygen ions from the high partial-pressure side to the low partial-pressure side without external electrical loadings. As no species other than oxygen ions are transferred, the oxides possess an infinite oxygen permselectivity. This unique characteristic makes them promising as a clean, efficient, and economical means of producing oxygen from air.

All the reported mixed oxygen ion and electron conducting ceramics are doped compounds, which can be largely classified into four categories based on the following oxides: (1) $Sr(Co,Fe)O_{3-\delta}$(SCF), (2) $La(Co,Fe)O_{3-\delta}$ (LCF), (3) $LaGaO_{3-\delta}$ (LGO), and (4) nonperovskite oxides. Among these categories, LCF-based oxides often exhibit much higher electronic conductivity than ionic conductivity. Therefore, the bulk ionic conduction is the rate-limiting factor for oxygen permeation (Kharton et al., 2000a). Conversely, $LaGaO_3$-based oxides show a lower electronic conductivity, but a much higher oxide-ion conductivity (Kharton et al., 2000b). A good mixed conducting membrane should exhibit both high and comparable electronic and ionic conductivities. Therefore, SCF-based oxides are exceptional for oxygen permeation and even the electronic conductivity is still a prevailing one (Kharton et al., 2000c). Nonperovskite-type oxides generally possess a better stability than the perovskite ones, but have poorer oxygen permeability (Bochkov et al., 1999). As discussed in most of the previous work, the preparation of mixed conducting materials with a high performance of oxygen permeation and a high stability is one of the most important subjects and has attracted considerable attention. One of the typical examples is the study of fluorite-type $Bi_{1.5}Y_{0.3}Sm_{0.2}O_3$ (BYS) and silver dual-phase membranes in which the continuous silver phase increases both the electronic conductivity and surface reaction rate, with the result of substantial improvement of oxygen permeance (Kim and Lin, 2000).

Most work in oxygen permeation through mixed-conducting ceramics was focused on the disk-shaped symmetric membranes because they are easy to fabricate using conventional sintering methods. However, such small disk-shaped membranes are capable of providing only a very limited area for oxygen permeation. Moreover, a high electrochemical transport resistance exists due to the symmetric structure of the membrane prepared. These drawbacks cannot be overcome, even using the dense tubular membranes prepared by the plastic extrusion or the isostatic pressing technique (Balachandran et al., 1995; Li et al., 2000). Success in fabrication of a dense hollow-fiber ceramic membrane with asymmetric structures using a combined sol–gel/phase inversion method provides the possibility of putting the mixed conducting

Correspondence concerning this article should be addressed to K. Li.

membrane to practical use (Luyten et al., 2000; Liu et al., 2000). Compared to the disk-shaped membrane, asymmetric hollow-fiber membranes possess many advantages, such as larger membrane area per unit volume, less membrane resistance to oxygen transfer, and improved sealing options (adopting a long hollow fiber and keeping the two sealing ends away from the high-temperature zone).

In this study, a mathematical model for air separation in a dense ceramic hollow-fiber module has been developed. Various factors affecting the performance of the module have been investigated theoretically. The perovskite oxide $La_{0.6}Sr_{0.4}Co_{0.2}F_{0.8}O_{3-\delta}$ (LSCF) has been selected as the membrane to investigate the performances of the module due to its high oxygen permeability and good chemical stability, as reported in the literature (Xu and Thomson, 1998).

Theory

Mechanism for oxygen permeation through a mixed ion-conducting membrane is schematically shown in Figure 1. The permeation process from the high oxygen partial-pressure side to the low oxygen partial-pressure side includes the following steps in series: (1) mass transfer of gaseous oxygen from the gas stream to the membrane surface (high-pressure side); (2) reaction between the molecular oxygen and oxygen vacancies at the membrane surface (high-pressure side); (3) oxygen vacancy bulk diffusion across the membrane; (4) reaction between lattice oxygen and electron-hole at the membrane surface (low-pressure side); and (5) mass transfer of oxygen from the membrane surface to the gas stream (low-pressure side). It has been shown that the gas-phase mass-transfer resistances (steps 1 and 5) are small and negligible (Xu and Thomson, 1999). Therefore, only the membrane bulk diffusion and the surface reactions are taken into consideration in this work.

Oxygen flux in the mixed conducting membrane

The transport fluxes of charged defects in mixed conductors at steady state under the electrochemical potential gradient can be expressed as (the full derivation is given in the Appendix)

$$J_i = -D_i C_i \left[\frac{1-t_i}{C_i} \cdot \frac{dC_i}{dx} - \sum_{j \neq i} \frac{z_i}{z_j} \cdot \frac{t_j}{C_j} \cdot \frac{dC_j}{dx} \right] \tag{1}$$

where D, C, z, t are the diffusivity, concentration, charge number, and the transport number of defect i, respectively.

As shown in Figure 1, the oxygen vacancy, $V_{\ddot{O}}$, and electron hole, $\dot{h}$, are the only mobile charged carried in the mixed conducting membrane (Xu and Thomson, 1999); Eq. 1 is therefore reduced to

$$J_V = -\frac{(C_h + 4C_V) D_V D_h}{C_h D_h + 4 C_V D_V} \cdot \frac{dC_V}{dx} \tag{2}$$

Furthermore, for the perovskite ceramic membranes whose ionic transference number closes to zero ($C_h D_h \gg C_V D_V$ and $C_h \gg C_V$) (Qiu et al., 1995; Kharton et al., 1996); Eq. 2 is further simplified as

$$J_V = -D_V \cdot \frac{dC_V}{dx} \tag{3}$$

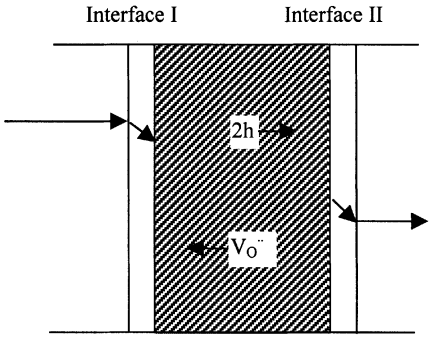

Figure 1. Oxygen permeation in a mixed ion-conducting membrane.

Based on the stoichiometric relations of oxygen and the oxygen vacancy, the oxygen flux can be written as

$$J_{O_2} = -\frac{1}{2} J_V \tag{4a}$$

or

$$J_{O_2} = \frac{D_V}{2} \cdot \frac{dC_V}{dx} \tag{4b}$$

Since D_V is generally considered to be a constant at a given temperature (Xu and Thomson, 1999), the local oxygen flux or molar flow rate for a hollow fiber can be written as

$$J_{O_2} = \frac{1}{2\pi r} \frac{dN_{O_2}}{dl} = \frac{D_V}{2} \frac{dC_V}{dr} \tag{5a}$$

or

$$dN_{O_2} = \pi D_V \frac{\int_{C_V'}^{C_V''} dC_V}{\int_{R_{in}}^{R_o} \frac{dr}{r}} dl = \pi D_V \frac{C_V'' - C_V'}{\ln \frac{R_o}{R_{in}}} dl \tag{5b}$$

where R_o and R_{in} are the outer and inner radius of the hollow fiber, respectively; the prime and double prime represent the high and low oxygen pressure sides of the membrane; and dl is an element of the hollow-fiber length.

On the membrane surfaces, the following reversible reactions take place at the high- and low-pressure sides, respectively

$$\frac{1}{2}O_2 + V_{\ddot{O}} \xleftrightarrow{k_f/k_r} O_O^x + 2\dot{h} \tag{6a}$$

$$O_O^x + 2\dot{h} \xleftrightarrow{k_f/k_r} \frac{1}{2}O_2 + V_{\ddot{O}} \tag{6b}$$

where O_O^x represents lattice oxygen in the perovskite crystal structure, and k_f and k_r are, respectively, the forward and reverse reaction rate constants for the surface reactions. It may involve many substeps, such as oxygen adsorption, dissociation, recombination, and charge transfer (van Hassel et al., 1993).

It should be noted that because of the high electronic conductivity, the electron holes are essentially constant at both surfaces of the membrane, and thus the reverse and forward reaction rates of the surface reactions of Eqs. 6a and 6b are pseudo zero-order at steady state under isothermal conditions (Xu and Thomson, 1999). Therefore, the local rate of oxygen consumed (step 2) or formed (step 4) in the hollow fiber can be, respectively, expressed in the following two equations if they are assumed to be elementary

$$dN_{O_2} = 2\pi R_o \left[k_f (p'_{O_2})^{0.5} C'_V - k_r \right] dl \qquad (7a)$$

$$dN_{O_2} = 2\pi R_{in} \left[k_r - k_f (p''_{O_2})^{0.5} C''_V \right] dl \qquad (7b)$$

where p'_{O_2} and p''_{O_2} are the partial pressures of oxygen at the hollow-fiber membrane outer and inner surfaces, respectively. Solving Eqs. 5 and 7 simultaneously, the local oxygen permeation rate in a hollow fiber can be correlated to the partial pressures of oxygen

$$dN_{O_2} = \frac{k_r \left[(p'_{O_2})^{0.5} - (p''_{O_2})^{0.5} \right]}{\frac{k_f \ln(R_o/R_{in})(p'_{O_2})^{0.5}(p''_{O_2})^{0.5}}{\pi D_V} + \frac{(p'_{O_2})^{0.5}}{2\pi R_{in}} + \frac{(p''_{O_2})^{0.5}}{2\pi R_o}} dl \qquad (8)$$

Models for hollow-fiber membrane module

The membrane module consists of n hollow fibers, in which are the operating flow patterns of cocurrent and countercurrent, as shown in Figure 2. Air is introduced into the shell side of the module at elevated pressures, while a vacuum is sometimes applied in the fiber lumen. With the different feed pressure or vacuum level applied, various oxygen permeate flow rates can be obtained.

In formulating the mathematical model, the following assumptions have been adopted:

1. The membrane module is operated at steady state under an isothermal condition.

2. The transport fluxes of charged defects are only in the radial direction of the hollow-fiber membrane, and are negligible in the axial direction because of the long hollow fibers used.

3. The gas-phase mass-transfer resistances are negligible. Therefore, oxygen partial pressures on the membrane surfaces are, respectively, equal to those in the module shell or lumen.

4. Ideal gas law is used to describe the gas behavior of a single-component and gas mixture.

5. The plug-flow conditions are attained in both gas streams, and the axial dispersion is negligible.

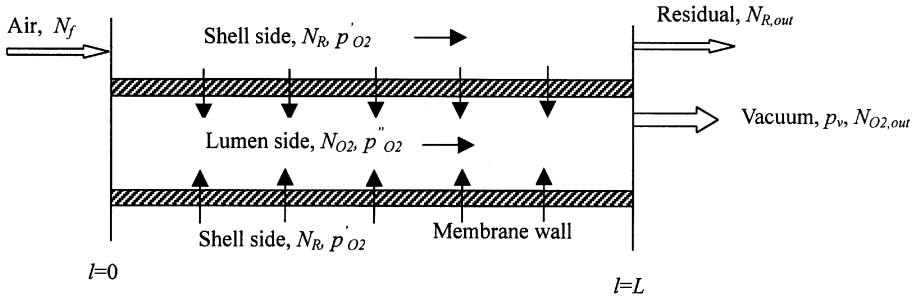

(a)

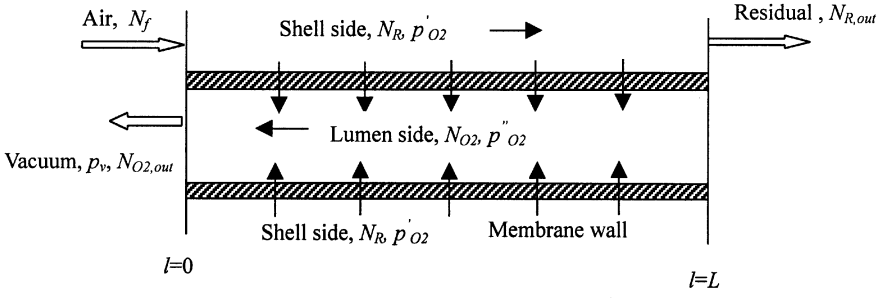

(b)

Figure 2. Operating modes: (a) cocurrent flow; (b) countercurrent flow.

Based on the preceding assumptions, the oxygen permeation equation derived in the preceding section, that is, Eq. 8, can be readily employed, while the overall and component material balances can be written based on operating flow patterns as shown in Figure 2, and are given as follows

Cocurrent Flow

$$\text{Overall: } N_f = N_{O_2} + N_R, \tag{9a}$$

$$O_2\text{: } 0.21N_f = N_R\frac{p'_{O_2}}{p} + N_{O_2} \tag{9b}$$

In addition, the Hagen–Poiseuille equation is employed to describe the pressure profile in the lumen

$$\frac{dp''_{O_2}}{dl} = -\frac{8\mu RT}{n\pi R_{in}^4 p''_{O_2}}\cdot N_{O_2} \tag{10}$$

Boundary conditions for this case are

$$l = 0,\ N_R = N_f,\ N_{O_2} = 0,\ p'_{O_2} = 0.21\ p,$$
$$l = L,\ p''_{O_2} = p_v$$

Countercurrent Flow

$$\text{Overall: } N_R = N_{R,out} + N_{O_2} \tag{11a}$$

$$O_2\text{: } N_R\frac{p'_{O_2}}{p} = N_{R,out}\frac{p'_{O_2,out}}{p} + N_{O_2} \tag{11b}$$

Again, the Hagen–Poiseuille equation is employed to describe the pressure profile in the lumen

$$\frac{dp''_{O_2}}{dl} = \frac{8\mu RT}{n\pi R_{in}^4 p''_{O_2}}\cdot N_{O_2} \tag{12}$$

Boundary conditions for this case are

$$l = 0,\ N_R = N_f,\ p'_{O_2} = 0.21p,\ p''_{O_2} = p_v,$$
$$l = L,\ N_{O_2} = 0$$

The preceding modeling equations derived for both the cocurrent and countercurrent flow patterns are a group of ordinary differential equations. Equations 8–10, describing the cocurrent flow, and Eqs. 8, 11, and 12, describing the countercurrent flow, are solved numerically using Runge–Kutta method.

Results and Discussion

Analysis of $La_{0.6}Sr_{0.4}Co_{0.2}F_{0.8}O_{3-\delta}$ (LSCF) hollow-fiber membranes for air separation was carried out theoretically. Values of the operating and the LSCF membrane parameters listed in Table 1 were employed in the calculations unless otherwise specified. The effects of process operating conditions and the characteristics of the membrane employed on oxygen permeation flux or productivity, α (defined as ratio of oxygen fed into the module to that produced ($\alpha = N_{O_2,out}/0.21N_f$), are analyzed and presented below. The results generated from the mathematical model developed were also compared with experimental data from the literature (Li et al., 2000).

Table 1. Parameters Used in the Simulation of the LSCF Hollow-Fiber Membrane Module

Membrane area*	$A_m = 200$, cm^2
OD of the hollow fiber	$d_o = 0.1$, cm
ID of the hollow fiber	$d_{in} = 0.05$, cm
Length of the reactor (hollow fiber)	$L = 20$, cm
Operating pressure in shell side	$p = 1$, atm
Vacuum pressure in fiber lumen	$p_v = 0.01$, atm
Operating temperature	$T = 1{,}173$, K
Feed flow rate	$N_f = 5$, cm$^3\cdot$s^{-1}
Diffusion coefficient of oxygen vacancy, cm$^2\cdot$s^{-1}	$D_v = 1.58\times10^{-2}\exp\left(-\frac{8852.5}{T}\right)$, (Xu and Thomson, 1999)
Forward reaction rate constant of Eq. 6a, cm$\cdot$atm$^{-0.5}\cdot$s^{-1}	$k_f = 5.90\times10^{6}\exp\left(-\frac{27291}{T}\right)$, (Xu and Thomson, 1999)
Reverse reaction rate constant of Eq. 6b, mol$\cdot$cm$^{-2}\cdot$s^{-1}	$k_r = 2.07\times10^{4}\exp\left(-\frac{29023}{T}\right)$, (Xu and Thomson, 1999)

*Defined as $A_m = 2n_p L\cdot\frac{R_o - R_{in}}{\ln(R_o/R_{in})}$

Effect of operating pressures and temperatures

Calculated values for these effects are given in Figures 3–5. In Figure 3, oxygen permeation flux is plotted against the vacuum pressure applied in the hollow-fiber lumen for different operating temperatures, while keeping the shell-side pressure at 1 atm. It can be seen from the figure that as the vacuum level is increased, the oxygen flux is improved, but

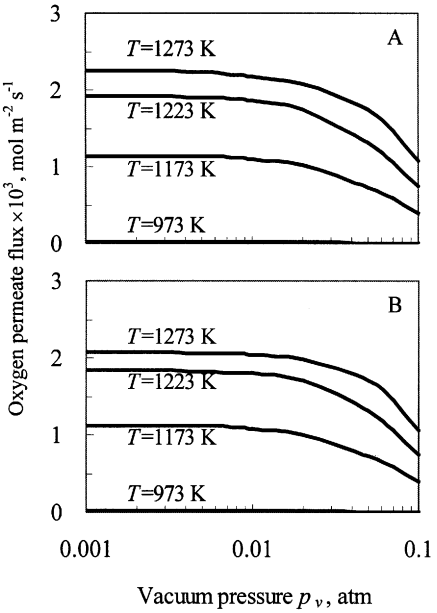

Figure 3. Effect of vacuum pressure on oxygen permeation flux ($p = 1$ atm): A: cocurrent; B: countercurrent.

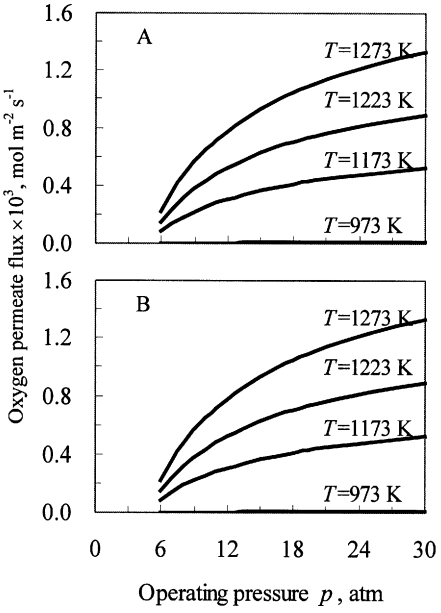

Figure 4. Effect of operating pressure on oxygen permeation flux ($p_v = 1$ atm): A: cocurrent; B: countercurrent.

only up to a certain value of the vacuum pressure, which may be termed the effective vacuum pressure. Any further increase in the vacuum level (decrease in the vacuum pressure) after this, effective vacuum pressure does not result in better oxygen permeation performance, as shown in the figure. This behavior is true for different operating temperatures and flow patterns, and it is interesting to note that the effective vacuum pressure, in this case about 0.01 atm, remains almost identical and does not seem to be dependent on the operating temperature and flow pattern.

In Figure 4, the effect of shell-side pressure on the oxygen permeation flux is shown for different operating temperatures, keeping the lumen-side pressure at 1 atm. As expected, elevation of the operating pressure in the shell side would generally increase the oxygen permeation flux. However, the trend of such an increase is clearly nonlinear, indicating that the mass-transfer resistance of the membrane is a function of the operating pressure applied. Further inspection of Figures 3 and 4 indicates that the LSCF hollow-fiber module operated at the elevated pressure may not be a better choice as compared to that operated at a vacuum condition. As can be seen from the calculated data, at an operating temperature of 1,273 K, the oxygen permeation flux of about 2.3×10^{-3} mol/m^2·s can be easily achieved when the vacuum pressure applied in the lumen side of the module is reduced to 0.01 atm (Figure 3). Such an oxygen permeation flux would not be possible to achieve at the elevated pressure operation; even the shell-side pressure is increased to 30 atm, as shown in Figure 4. It thus follows that the elevated pressure operation commonly employed in the conventional polymeric hollow-fiber membrane modules for gas separation is not suitable for the LSCF hollow-fiber module. Instead, the vacuum operation in the lumen side of the membrane module would be preferable, as it yields much higher oxygen production rates.

The effect of the operating temperature on the oxygen permeation is shown in Figure 5, where the oxygen productivity is plotted against the temperature. It can be seen that the oxygen productivity is less than 0.1 at an operating temperature of 1,000 K or lower. Oxygen production increases drastically after 1,000 K, and then approaches its maximum value at 1,300 K for $A_m = 0.02$ m^2, at 1,180 K, for $A_m = 0.05$ m^2, and at 1,130 K for $A_m = 0.1$ m^2, respectively. The results indicate that the membrane area plays an important role in the production of oxygen. For a given module, that is, membrane area, the optimum production of oxygen can be achieved with careful selection of operating pressure and temperatures, as illustrated in the preceding three figures.

Effect of flow patterns

Predicted values for this effect are given in Figures 6 and 7. In Figure 6, the vacuum level in the hollow-fiber lumen is plotted against oxygen productivity, α, for both the cocurrent and countercurrent flow patterns. It can be seen that cocurrent flow exhibits higher oxygen productivity compared to the countercurrent flow pattern when the vacuum pressure is less than 0.05 atm. When the vacuum pressure is higher than 0.05 atm, the difference between two flow patterns becomes small. This is clear in comparison to the results for a polymeric hollow-fiber membrane module, where the countercurrent flow pattern always leads to better separation. Such contrary be-

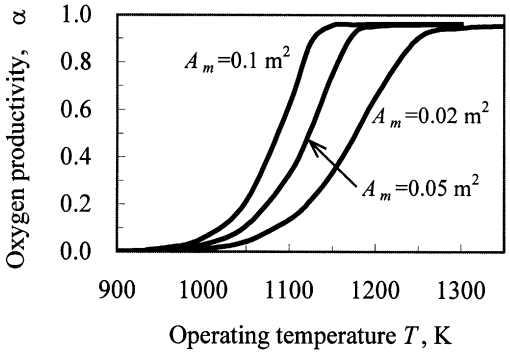

Figure 5. Effect of operating temperature on oxygen productivity.

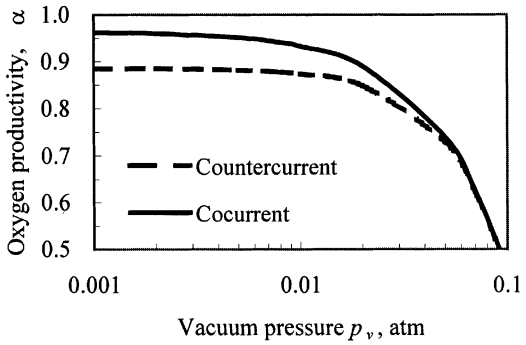

Figure 6. Cocurrent vs. countercurrent flow patterns ($T = 1{,}273$ K).

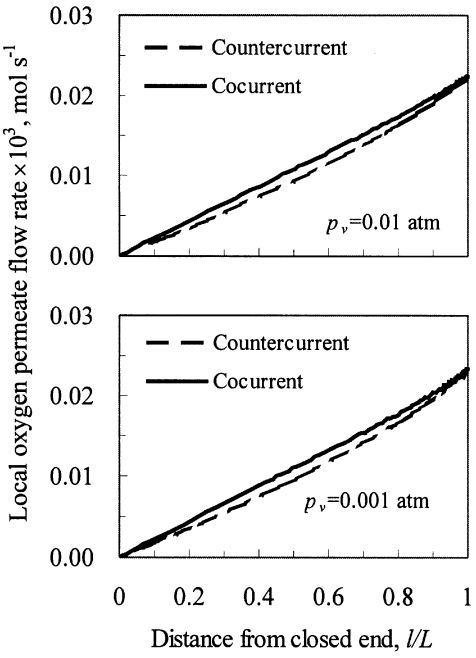

Figure 7. Local oxygen permeate flow rate for cocurrent and countercurrent flow patterns.

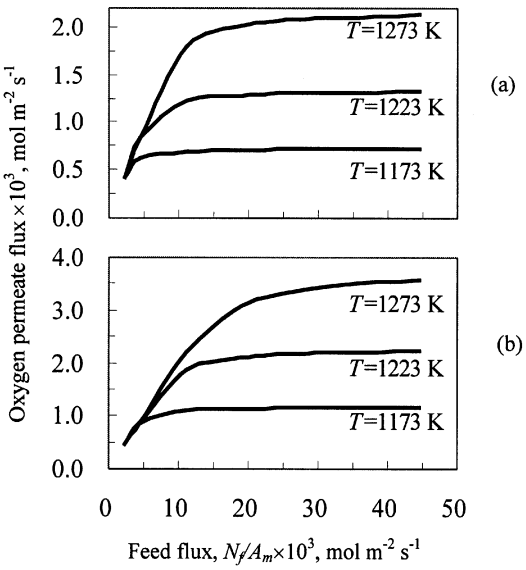

Figure 8. Effect of feed flow rate on oxygen permeation flux: (a) p = 20 atm, p_v = 1 atm; (b) p = 1 atm, p_v = 0.01 atm.

havior is due to the high local oxygen permeation available in the module for the cocurrent flow pattern. As illustrated in Figure 7, profile of the local permeation flow of oxygen for the cocurrent flow pattern is always greater than that for the countercurrent flow pattern throughout the entire hollow-fiber length, thus resulting in high oxygen productivity. Therefore, the cocurrent flow pattern has been used in all the subsequent simulation studies.

Effect of feed flow rate

The effect of the feed flow rate for a given membrane area on the oxygen permeation flux is illustrated in Figure 8. As can be seen, the oxygen permeation flux increases as the feed flow rate is increased, but only up to 12×10^{-3} mol/m^2·s, beyond which the oxygen permeation flux remains relatively unchanged, as shown in Figure 8a. Because hydrodynamics of the feed flow provides a negligible effect on the oxygen permeation, due to the dominance of the membrane resistance, the dependence of the oxygen flux at a lower feed flow rate is due to the change in the oxygen driving force. At a feed flow rate of 20×10^{-3} mol/m^2·s or greater, the partial pressure of oxygen in the shell side remains constant (close to 0.21) throughout the module, and hence the maximum value of the oxygen permeation flux is attained. It should be noted that for the vacuum-pressure operation, such a maximum oxygen permeation flux could not be reached unless the feed flow rate is further increased to 25×10^{-3}–40×10^{-3} mol/m^2·s, as shown in Figure 8b. The reason for this difference is probably due to the high oxygen permeation flux achievable under vacuum-pressure operation. With the increased permeation characteristics, the maximum oxygen permeation flux could only be achieved by a further increase in the feed flow rate.

Effect of membrane area

As illustrated earlier, the operating pressure, p, in the shell side of the module and the vacuum pressure, p_v, in the fiber lumen determine the oxygen permeation flux for a given membrane module. If the pressure buildup in the fiber lumen is negligible, the maximum oxygen productivity, α_{max}, can be derived from Eq. 9 with a condition that partial-pressure oxygen in the shell side of the module is equal to that in the lumen, that is, $p'_{O_2} = p_v$ as

$$\alpha_{max} = \frac{p - p_v/0.21}{p - p_v} \tag{13}$$

Figure 9 illustrates the effect of the membrane area on the oxygen productivity at different vacuum pressures, keeping the shell-side pressure and operating temperature at 1 atm and 1173 K, respectively. The dashed lines in Figure 9 are the maximum oxygen productivities obtained from Eq. 13 for

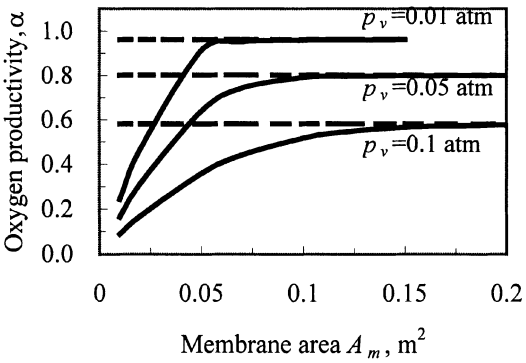

Figure 9. Effect of membrane area on the oxygen productivity.

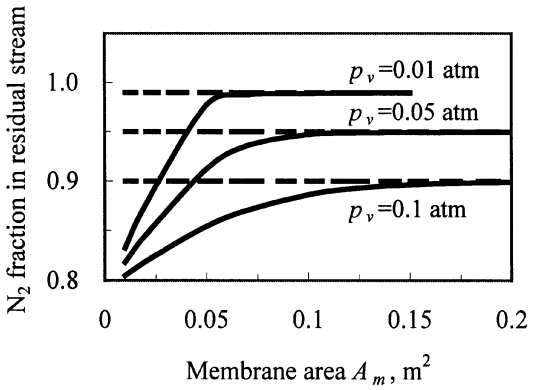

Figure 10. Effect of membrane area on the nitrogen purity in the residual stream.

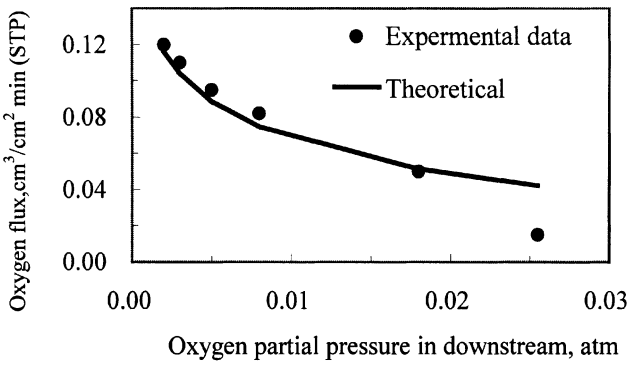

Figure 11. Permeation flux of oxygen at various downstream oxygen partial pressures at the temperature of 1,123 K ($p = 1$ atm).

the different vacuum pressures. It can be seen that for a given feed flow rate, the oxygen productivity increases as the membrane area is increased. However, further increase in the membrane area would result in no effect once the maximum value of the oxygen productivity is reached. It is interesting to note that the higher the vacuum level, the less the membrane area required to achieve the high oxygen productivity. This therefore suggests that economically there is a trade-off between the vacuum level and membrane area required to obtain optimum pure-oxygen production.

The membrane employed in this study has the absolute selectivity to oxygen; hence, the pure-oxygen product is achievable in the permeate side of the module. However, the purified nitrogen in the residual side is not simultaneously achieved, as the oxygen in air would not be entirely permeated unless an absolute vacuum is applied in the fiber lumen, as shown in Figure 10. In addition, a desired membrane area must also be provided for a given feed flow rate. As a result, the high vacuum level as well as enough membrane area is essential to produce the pure oxygen and nitrogen simultaneously.

Comparison with experimental data

Although there are so far many studies on oxygen permeable ceramic materials, very limited experimental work on membrane modules for air separation has been conducted. Li et al. (2000) performed some experiments on oxygen permeation through a tubular LSCF membrane, the dimensions of which were 8 mm in outer diameter, 15 cm in length, and 1.5 mm in wall thickness. Air was introduced into the shell side of the module. Helium used as a sweep gas was fed to the bore of the tube. Both upstream and downstream were maintained at atmospheric pressures. The partial pressure of oxygen in the bore side of the tube was maintained by adjusting the flow rate of helium. Figures 11 and 12 compare the experimental results with the theoretical values calculated based on the models developed in this study. In Figure 11, the oxygen permeation flux is plotted against the oxygen partial pressures in the bore side at the temperature of 1,123 K, while the oxygen partial pressure in the shell side was kept at a constant value, that is, 0.21 atm. As can be seen, all the oxygen permeation fluxes, except for one point at the highest oxygen partial pressure, are in good agreement with the calculation results predicted using kinetic parameters given by Xu and Thomson (1999).

Figure 12 plots the oxygen permeation through the membrane at different operating temperatures while keeping the partial pressures of oxygen in the shell and bore sides at 0.21 atm and 0.001 atm, respectively. The increasing trend of oxygen permeation with temperature is also in good agreement with the modeling results. However, the theoretical results show some deviations at a temperature above 1,073 K, where experimental results reflected distinctly the order–disorder transition of the oxygen vacancy (Li et al., 2000), which is not predictable by the model. Nevertheless, the comparisons given in Figures 11 and 12 indicate the theoretical model developed in this study, together with the kinetic parameters given by Xu and Thomson (1999), can be used with confidence to predict the performances of the hollow-fiber LSCF membranes for oxygen separation from air.

The simulation results and experimental data under different helium flow rates and operating temperatures are also shown in Figure 13. As expected, the oxygen fluxes increase with the increasing helium flow rate, because the oxygen partial pressure in the downstream decreases as the helium flow rate is increased, giving an increased driving force for oxygen

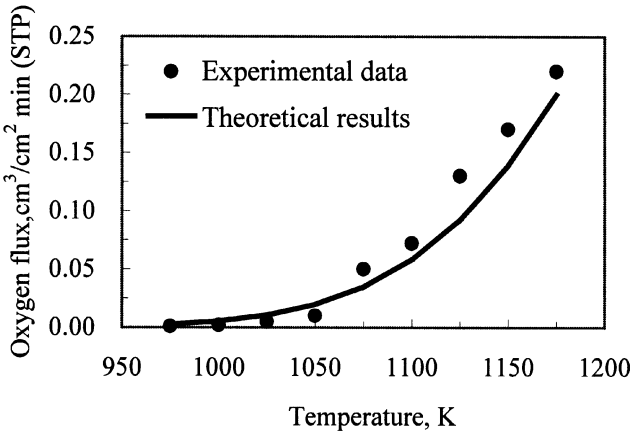

Figure 12. Temperature dependence of the oxygen permeation flux ($p'_{O_2} = 1$ atm, $p''_{O_2} = 0.001$ atm).

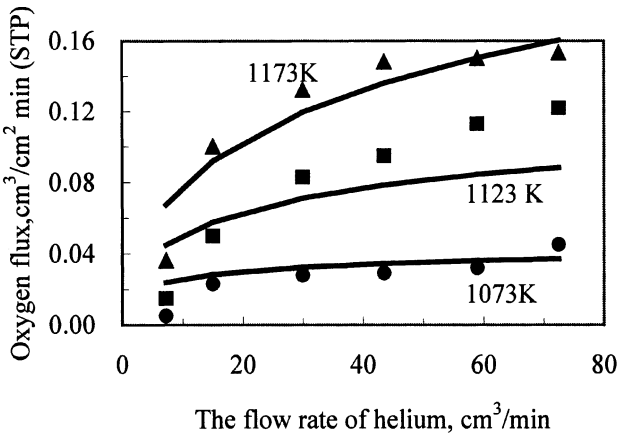

Figure 13. Helium flow-rate dependence of the oxygen permeation in a tubular LSCF membrane (air flow rate: 200 mL/min): ●: 1,073 K; ■: 1,123 K; ▲: 1,173 K.

permeation. In the theoretical analysis, the area used to perform the calculation was only about 40% of the experimental value given by Li et al. (2000). Such a difference in the membrane area may be due to the configuration of the membrane module design, where the effective area available for oxygen permeation is considerably less than the actual area employed. Meanwhile, it is seen that all the experimental data at lower helium flow rates are much less than theoretical results, possibly due to the mass-transfer resistance in the gas phase, which may play a role in the oxygen permeation under such operating conditions.

Conclusions

A mathematical model has been developed for a ceramic hollow-fiber membrane module for the cases of cocurrent and countercurrent operating conditions. The problem of air separation in a mixed ion conducting $La_{0.6}Sr_{0.4}Co_{0.2}F_{0.8}O_{3=\delta}$ (LSCF) membrane has been considered in the simulation. The results indicate that the cocurrent flow pattern is advantageous over the countercurrent flow pattern, and the vacuum operation in the lumen side of the membrane module is preferable for higher oxygen productivity compared to the elevated pressure operation in the shell side. In addition to the operating temperature, a high vacuum level and the desired membrane area are essential for producing pure oxygen and nitrogen simultaneously. Experimental results and kinetic parameters in the literature obtained from the LSCF modules with different dimensions for air separation are in satisfactory agreement with the theoretical solutions.

Acknowledgments

The authors gratefully acknowledge the research funding provided by EPSRC in the United Kingdom (Grant No. GR/N38640).

Notation

A_m = membrane area, cm^{-2}
C_i = concentration of defect i, $mol \cdot cm^{-3}$
C'_V = vacancy concentration at upstream gas
C''_V = vacancy concentration at downstream gas
D_i = effective diffusivity of defect i, $cm^2 \cdot s^{-1}$
J_i = transport flux of defect i, $mol \cdot cm^{-2} \cdot s^{-1}$
J_{O_2} = oxygen flux across membrane, $mol \cdot cm^{-2} \cdot s^{-1}$
k_r = reverse reaction rate constant of Eq. 6, $mol \cdot cm^{-2} \cdot s^{-1}$
k_f = forward reaction rate constant of Eq. 6, $cm \cdot atm^{-0.5} \cdot s^{-1}$
l = length variable of hollow-fiber membrane module, cm
L = length of hollow-fiber membrane module, cm
n = number of hollow-fiber membranes
N_f = feed flow rate of air, $mol \cdot s^{-1}$
N_R = molar flow rate of residual, $mol \cdot s^{-1}$
$N_{R,out}$ = molar flow rate of residual at exit of the module, $mol \cdot s^{-1}$
N_{O_2} = molar flow rate of oxygen in fiber lumen, $mol \cdot s^{-1}$
$N_{O_2,out}$ = molar flow rate of oxygen at exit of the module, $mol \cdot s^{-1}$
p = operating pressure at shell side, atm
p'_{O_2} = oxygen partial pressure at upstream, atm
p''_{O_2} = oxygen partial pressure at downstream, atm
p_v = vacuum pressure in the fiber lumen, atm
p_{O_2} = oxygen partial pressure, atm
r = radius variable of hollow fiber, cm
R = gas constant, 82.06 $atm \cdot cm^3 \cdot mol^{-1} \cdot K^{-1}$
R_{in} = inner radius of hollow fiber, cm
R_o = outer radius of hollow fiber, cm
t_i = transport number of defect I
T = operating temperature, K
x = membrane thickness variable, cm
z_i = charge number of defect I

Greek letters

α = oxygen productivity, $\alpha = N_{O_2}/0.21N_f$
α_{max} = the limit oxygen productivity
μ = oxygen viscosity, $g \cdot cm^{-1} \cdot s^{-1}$

Literature Cited

Balachandran, U., J. T. Dusk, R. L. Mieville, R. B. Poeppel, M. S. Kleefisch, S. Pei, T. P. Kobylinski, C. A. Udovich, and A. C. Bose, "Dense Ceramic Membranes for Partial Oxidation of Methane to Syngas," *Appl. Catal. A: Gen.*, **133**, 19 (1995).

Bochkov, D. M., V. V. Kharton, A. V. Kovalevsky, A. P. Viskup, and E. N. Naumovich, "Oxygen Permeability of $La_2Cu(Co)O_{4+\delta}$ Solid Solutions," *Solid State Ionics*, **120**, 281 (1999).

Goto, K. S., *Solid State Electrochemistry and Its Applications to Sensors and Electronic Devices*, Elsevier, Amsterdam (1988).

Kim, J., and Y. S. Lin, "Synthesis and Oxygen Permeation Properties of Ceramic-Metal Dual-Phase Membranes," *J. Memb. Sci.*, **167**, 123 (2000).

Kharton, V. V., E. N. Naumovich, A. V. Kovalevsky, A. P. Viskup, F. M. Figueiredo, I. A. Bashmakov, and F. M. B. Marques, "Mixed Electronic and Ionic Conductivity of $LaCo(M)O_3$ (M = Ga, Cr, Fe or Ni) IV. Effect of Preparation Method on Oxygen Transport in $LaCoO_{3-\eta}$," *Solid State Ionics*, **138**, 135 (2000a).

Kharton, V. V., A. P. Viskup, A. A. Yaremchenko, R. T. Baker, B. Gharbage, G. C. Mather, F. M. Figueiredo, E. N. Naumovich, and F. M. B. Marques, "Ionic conductivity of $La(Sr)Ga(Mg,M)O_{3-\delta}$ (M = Ti, Cr, Fe, Co, Ni): Effects of Transition Metal Dopants," *Solid State Ionics*, **132**, 119 (2000b).

Kharton, V. V., A. P. Viskup, A. V. Kovalevsky, J. R. Jurado, E. N. Naumovich, A. A. Vecher, and J. R. Frade, "Oxygen Ionic Conductivity of Ti-Containing Strontium Ferrite," *Solid State Ionics*, **133**, 57 (2000c).

Kharton, V. V., E. N. Naumovich, and A. V. Nikolaev, "Materials of High-Temperature Electrochemical Oxygen Membranes," *J. Memb. Sci.*, **111**, 149 (1996).

Li, S. G., W. Q. Jin, P. Huang, N. P. Xu, J. Shi, and Y. S. Lin, "Tubular Lanthanum Cobaltite Perovskite Type Membrane for Oxygen Permeation," *J. Memb. Sci.*, **166**, 51 (2000).

Liu, S., X. Tan, K. Li, and R. Hughes, "Preparation and Characterization of $SrCe_{0.95}Yb_{0.05}O_{2.975}$ Hollow-Fibre Membranes," **193**, 249 (2001).

Luyten, J., A. Buekenhoudt, W. Adriansens, J. Cooymans, H. Weyten, F. Servaes, and R. Leysen, "Preparation of $LaSrCoFeO_{3-\chi}$ Membranes," *Solid State Ionics*, **135**, 637 (2000).

Qiu, L., T. H. Lee, L.-M. Liu, Y. L. Yang, and A. J. Jacobson, "Oxygen Permeation Studies of $SrCo_{0.8}Fe_{0.2}O_{3-\delta}$," *Solid State Ionics*, **76**, 321 (1995).
Van Hassel, B., A. Kawada, T. Sakai, N. Yokokawa, H. Dokiya, and H. J. M. Bouwmeester, "Oxygen Permeation Modeling of Perovskites," *Solid State Ionics*, **66**, 295 (1993).
Xu, S. J., and W. J Thomson, "Stability of $La_{0.6}Sr_{0.4}Co_{0.2}Fe_{0.8}O_{3-\delta}$ Perovskite Membrane in Reducing and Nonreducing Environments," *Ind. Eng. Chem. Res.*, **37**, 1290 (1998).
Xu, S. J., and W. J. Thomson, "Oxygen Permeation Rates Through Ion-Conducting Perovskite Membranes," *Chem. Eng. Sci.*, **54**, 3839 (1999).

Appendix

The flux of charged species in a conductor is described by the Nernst–Planck equation (Goto, 1988), which is a combination of Fick's law and the equation for ion migration

$$J_i = -\frac{\sigma_i}{z_i^2 F^2}\nabla\mu_i + C_i\boldsymbol{v} \tag{A1}$$

where σ_i, μ_i, $\boldsymbol{v}$ are the conductivity, electrochemical potential, and local velocity of the inert marker, respectively. The electrochemical potential for each charged species consists of a chemical potential or an activity term and a local electrostatic potential, ϕ

$$\mu_i = \mu_i^0 + RT\ \ln\ a_i + z_i F\phi \tag{A2}$$

where μ_i^0 and a_i are the standard chemical potential and activity, respectively.

For the general case, the local velocity of the inert marker is negligible, and a one-dimensional model is applicable in expressing the defect fluxes in the conductor with a small area. Therefore

$$J_i = -\frac{\sigma_i}{z_i^2 F^2}\left[RT\frac{\mathrm{d}\ln a_i}{\mathrm{d}x} + z_i F\frac{\mathrm{d}\phi}{\mathrm{d}x}\right] \tag{A3}$$

The conductivity of the defect, which is a measure of the random motion of the species i in the lattice by the Nernst–Einstein equation, can be correlated with its concentration and diffusivity

$$\sigma_i = \frac{z_i^2 F^2}{RT} C_i D_i \tag{A4}$$

In addition, when no external current is imposed on the membrane, the following correlation applies at steady state

$$\sum_i z_i J_i = 0 \tag{A5}$$

The electroneutrality condition also gives the relationship between the defect concentration gradients as

$$\sum_i z_i \cdot \frac{dC_i}{dx} = 0 \tag{A6}$$

With the given assumptions, rearranging Eqs. A3 to A6 yields the flux of charged species of Eq. 1.

Manuscript received Sept. 4, 2001, and revision received Jan. 4, 2002.